Backscattering Decay Processes in Electron Beam-Plasma Interactions Including Ion Dynamics*

B. H. Quon, A. Y. Wong, and B. H. Ripin†
Department of Physics, University of California, Los Angeles, California 90024
(Received 10 December 1973)

Electron plasma waves driven unstable by the electron beam-plasma instability are observed to decay into convectively and absolutely growing ion waves and electron waves propagating in opposite directions. Ion waves excited to large amplitudes further couple with the high-frequency unstable waves to produce nonresonant short-wavelength electron modes. The nonresonant modes are found effective in accelerating electrons and thermalizing the beam.

We wish to report experiments in a large, unmagnetized, electron beam-plasma system in which ion dynamics produce nonlinear interactions significantly different from previous experiments.[1] The high-frequency waves driven unstable by the beam first grow spatially, and then parametrically decay into ion waves and electron waves propagating in opposite directions. This backscattering process allows the parametrically excited ion waves to grow both spatially and temporally and resembles the backscattering processes[2] currently investigated in laser-plasma interactions. The large-amplitude ion waves ($n_1/n_0 \sim 10\%$) further couple with the initially unstable electron waves to produce nonresonant short-wavelength electron modes. These nonresonant modes traveling at $\frac{1}{3}$ beam velocity are effective in accelerating the background electrons and bringing about the merging of the beam and background electrons. Thus the description of the nonlinear process and the mechanism of the beam thermalization observed here requires the inclusion of ion dynamics.

The experiments are performed in the University of California, Los Angeles, double-plasma device[3] modified by adding an anode grid in front of the separation grid. The device enables the production of a gentle bump electron beam of a desired energy throughout the large diameter (30 cm) of the system. The axial dimension is 70 cm, allowing the beam to traverse the homogeneous plasma in about a hundred plasma periods (ω_{pe}^{-1}). Axially movable grid probes and disk probes are used to detect the wave signals and the electron current characteristics, whose derivatives yield a measure of the electron velocity distribution. A high-impedance probe ($R > 10\ k\Omega$, $Q \sim 150$) is constructed to measure the absolute wave potentials of the excited electron waves. Typical parameters are $n_e \sim 5\times 10^8\ \mathrm{cm}^{-3}$, $T_e/T_i \sim 15$, $n_b/n_e \sim 5$–10%, $v_e = (KT_e/m_e)^{1/2} \sim 6\times 10^7$ cm/sec, $v_B/v_e \sim 1$, and $v_d/v_e \sim 4$–5, where v_B is the beam velocity spread and v_d is the beam velocity. The plasma is produced from argon at pressure $p \sim 10^{-4}$ Torr.

The presence of the electron beam gives rise to the growth of a spontaneous noise[4] as shown in Fig. 1. The noise, peaking at $\omega \sim \omega_{pe}$, grows exponentially for 6–7 cm, then saturates at an amplitude 40–50 dB above the initial level. In the exponential growth region, there is a slow change in the electron distribution caused by the diffusion of beam electrons to slightly slower velocities. After the most unstable waves saturate the 3 dB width of the noise spectrum broad-

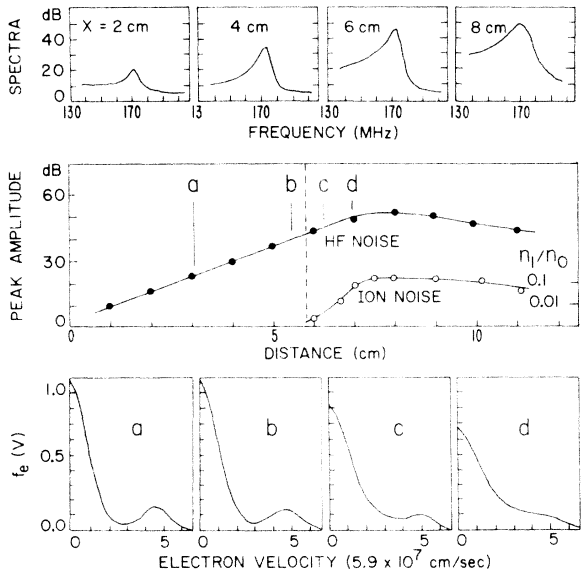

FIG. 1. The correlation between the high-frequency unstable noise and the evolution of the beam-plasma electron distribution function. Ion noises are generated in the saturation region via a parametric decay process.

ens from $\Delta\omega/\omega_{p_e} \sim 0.05$ to $\Delta\omega/\omega_{p_e} \sim 0.1$. In this region an ion-acoustic noise peaking at $\omega \sim 0.5\omega_{p_i}$ is generated and rapidly enhanced to $n_1/n_0 \sim 0.1$. Rapid changes in the electron distribution function occur when the ion noise is sufficiently developed. There a large amount (10–15%) of the background electrons are accelerated to velocities higher than the initial electron thermal speed. The accelerated electrons eventually fill up the space between the background electrons and the beam, forming a monotonically decreasing distribution function. The entire noise spectrum thereafter reaches a stable state and then decays gradually.

In order to identify the nonlinear process we apply a small (10–50 mV) tone burst of rf signal on the separation grid so that the spatial and temporal development of a selected mode can be followed closely. The wavelength and the spatial growth rate of the test wave are obtained by using an interferometric method. The linear dispersion relation measured is in good qualitative agreement with a theoretical calculation given by O'Neil and Malmberg,[5] identifying the initial instability to be a "bump in tail" type (Fig. 2). The most unstable waves satisfy the relations $\omega^2 \sim \omega_{p_e}^2 + 3\,k^2 v_e^2$, $k \sim \omega/v_d$, with the maximum spatial growth rates $k_i/k_r \sim 0.2$. These waves decay into sideband electron waves and ion-acoustic waves near the saturation region. Figure 3(a) shows the typical spectra and wave forms of the pump (test wave), the sideband, and the ion-acoustic waves. The wave forms and the direction of propagations of these waves are obtained by using two-probe spatial-correlation measurements. For high-frequency waves, signals monitored by a fixed and a movable probe are heterodyned to a

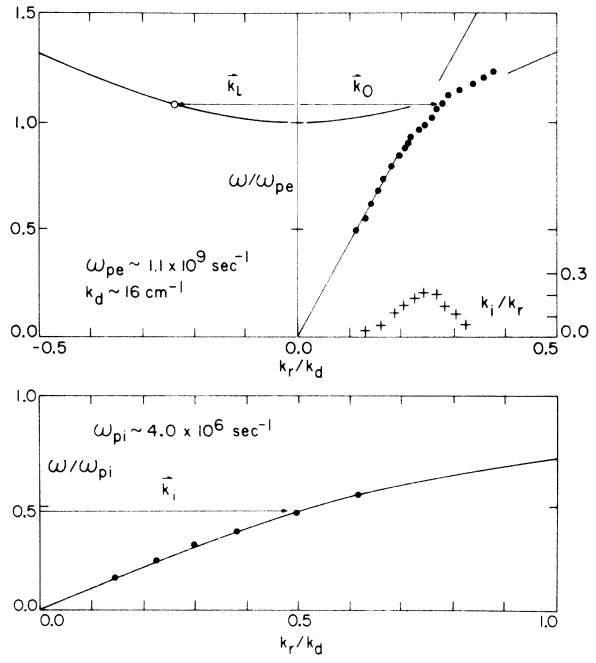

FIG. 2. Linear dispersions of the unstable electron waves and ion acoustic waves. Diagram indicates the backscattering selection rule: $\vec{k}_i = 2\vec{k}_0\vec{k}_L = -\vec{k}_0$, where $\vec{k}_0$, $\vec{k}_i$, and $\vec{k}_L$ are the wave numbers of the initially unstable jump, ion acoustic, and electron sideband waves, respectively.

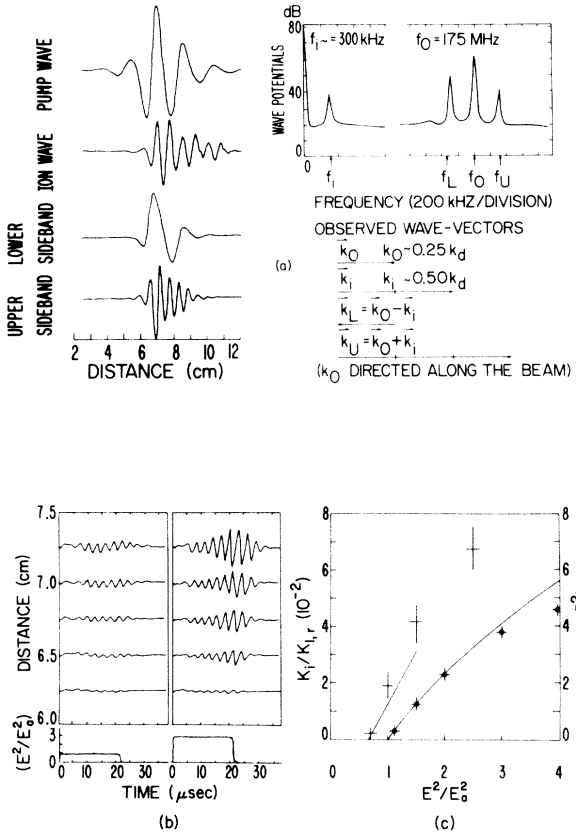

FIG. 3. (a) A measurement on the matching conditions $\omega_0 = \omega_i + \omega_L$ and $\vec{k}_0 = \vec{k}_i + \vec{k}_L$. Directions of $\vec{k}_i$ and $\vec{k}_L$ are deduced from the sense of the phase shifts with change in separation between two measuring probes. (b) Convective (left) and absolute (right) growth of ion waves generated by a tone-burst high-frequency pump wave in the saturation region. rf frequency $f_0 \simeq 175$ MHz. Ion wave frequency $f_1 \simeq 300$ kHz. Wave forms are measured by using a sampling scope. (c) The measured spatial (crossbars) and temporal (points) growth rates of the parametrically excited ion waves as functions of E^2/E_a^2, where E is the electrostatic field of the pump wave, E_a is the absolute threshold, and $E_a \sim 1.3 \pm 0.5$ V/cm.

lower radio-frequency range by the same local oscillator. The converted signals are then fed into two identical sharply tuned rf receivers whose bandwidths are small compared with the sideband separations. By tuning the local oscillator frequency, the wave vectors of the pump wave, lower-sideband wave, and upper-sideband wave can be measured separately. The observed wave numbers, $\vec{k}_0 \simeq 0.25 k_d \hat{e}$ (initially unstable mode), $\vec{k}_i \simeq 2\vec{k}_0$ (ion mode), and $\vec{k}_L \simeq -\vec{k}_0$ (lower sideband), where $\hat{e}$ is the direction of the electron beam, indicate that the decay process is indeed a backscattering type.[6]

The fact that the sideband wave and the ion wave have opposite group velocities should lead to the parametric instability of the absolute type.[7] This is experimentally verified by applying a tone burst of high-frequency signal on the separation grid so that the unstable pump wave starts at a known time. The spatial and temporal developments of the ion waves are observed as shown in Fig. 3(b). When the electrostatic field E of the pump wave is slightly above the convective threshold E_c, only spatial growth of the ion wave is observed. There is a measurable absolute threshold, $E_a^2/E_c^2 = 1.5 \pm 0.3$, above which the amplitude at a given location increases exponentially in time. The spatial and temporal growth rates of ion waves as functions of the relative pump wave power are plotted in Fig. 3(c). By using the high-impedance probe the convective threshold $E_c = 1.1 \pm 0.3$ V/cm is measured (in a cw excitation). This compares well with the theoretical value $E_c^2/4\pi n T_e \sim 4(\gamma_i/\omega_i)(\gamma_L/\omega_L)$, which gives $E_c \sim 0.9$ V/cm for the measured damping rates[8] $\gamma_i/\omega_i \sim 1.2\times 10^{-2}$, $\gamma_L/\omega_L \sim 1.6\times 10^{-2}$, and $k_0\lambda_d = 0.27$. The temporal growth rate is calculated as outlined by Fried, Gould, and Schmidt as[9]

$$\frac{\gamma}{\omega_i} \sim \frac{\gamma_i|V_L| + \gamma_L V_i}{\omega_i(V_i + |V_L|)}\left[\left(\frac{E^2}{E_a^2}\right)^{1/2} - 1\right] \sim 5.6\times 10^{-2}\left[(E^2/E_a^2)^{1/2} - 1\right],$$

and the absolute instability threshold is given by

$$E_a^2/E_c^2 \sim (L_i + L_L)^2/4L_iL_L \sim 1.5.$$

Here $V_{i,L}$ are the group velocities, and $L_{i,L} = |V_{i,L}|/\gamma_{i,L}$ are the damping lengths of the ion wave and the lower-sideband electron wave, respectively. The observed temporal growth rates remarkably coincide with the theoretical curve for E^2 just above E_a^2 [Fig. 3(c)].

A very interesting observation in our experiments is the generation of nonresonant, short-wavelength electron modes. From Fig. 3(a), the upper-sideband wave is measured to propagate with $v_{ph} = \frac{1}{3}v_d$ and does not satisfy the linear dispersion for Langmuir waves. It is driven by the high-frequency unstable pump wave (ω_0, k_0) and the ion density-fluctuation (ω_i, k_i) via a nonresonant mode-coupling process.[10] Using Poisson's equation together with the equation of continuity and the linearized equation of motion, we have derived for the upper-sideband wave $(\vec{k}_U = \vec{k}_0 + \vec{k}_i \sim 3\vec{k}_0)$

$$\ddot{E}_{k_U} + \gamma_e \dot{E}_{k_U} + (\omega_p^2 + 3k_U^2 v_e^2)E_{k_U} \sim 4\pi e \partial(n_{k_i} v_{k_0})/\partial t,$$

where γ_e is the phenomenological damping, n_{k_i} are the electron density fluctuations due to the ion wave, and v_{k_0} is the electron velocity perturbation caused by the pump wave. Using $\dot{v}_{k_0} \sim -(e/m)E_{k_0}$ and $k_0 \sim \omega_0/v_d$, we obtain

$$E_{k_U} \sim -\frac{1}{24}\frac{v_d^2}{v_e^2}\frac{n_{k_i}}{n_0}E_{k_0} \sim \frac{n_{k_i}}{n_0}E_{k_0}$$

for $v_d \sim (4-5)v_e$ and a measured damping rate $\gamma_e/\omega_p \sim 0.1$. The measured values $n_{k_i}/n_0 \sim 0.1$ and $E_{k_U} \sim 0.1E_{k_0}$ agree with this calculation. Since this mode has phase velocity comparable to the electron thermal velocity and should be strongly Landau damped, it is expected to have a large effect on particle acceleration. As a further check on the role of the ion-acoustic wave we introduce a small amount (0.5%) of He into the argon plasma, which suppresses the ion waves by increasing Landau damping. It is observed that the upper sideband is also suppressed simultaneously (Fig. 4). The electron velocity distribution shows that a large amount of electrons near the phase velocity of this mode disappear and the initial bump-on-tail distribution reappears. This effect indicates that the nonresonant electron modes are efficient in accelerating electrons and thermalizing the beam.

In conclusion, our experiments demonstrate the importance of ion dynamics[11] even for electron beam velocities much faster than the phase velocities of the ion-acoustic waves. The interactions between high- and low-frequency waves lead to nonlinear Landau damping[12] which are effective in the thermalization of the beam.

The authors would like to thank Dr. R. Stenzel, Professor B. Fried, and Professor J. Dawson for many helpful discussions. The experienced technical assistance of Mr. Z. Lucky and the

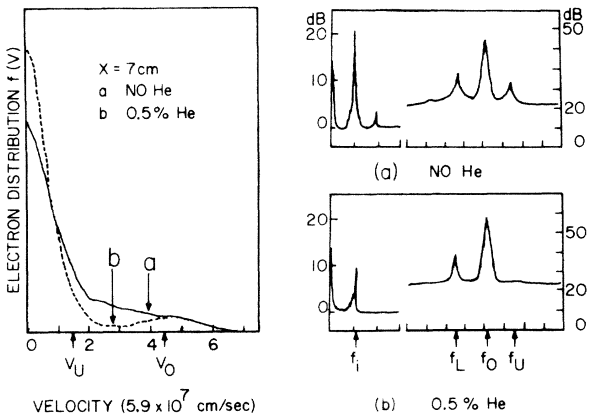

FIG. 4. Effects of the nonresonant upper-sideband mode $\omega_U = \omega_0 + \omega_i$, $\vec{k}_U = \vec{k}_0 + \vec{k}_i$ on the electron distribution (a) before adding He and (b) after 0.5% of He is added. Here V_0 is the phase velocity of the pump wave and V_U that of the upper-sideband wave.

participation of Mr. J. Matsumoto are gratefully acknowledged.

*Research supported by the National Science Foundation under Grant No. GP-38673X.

†Present address: Naval Research Laboratory, Washington, D. C. 20390.

[1]J. H. Malmberg and C. B. Wharton, Phys. Fluids 12, 2600 (1969); C. Roberson, K. W. Gentle, and P. Nielson, Phys. Rev. Lett. 26, 266 (1971); W. Carr, D. Boyd, H. Lin, G. Schmidt, and M. Seidl, Phys. Rev. Lett. 28, 662 (1972).

[2]M. Gorbunov, Zh. Eksp. Teor. Fiz. 55, 2298 (1968) [Sov. Phys. JETP 28, 1220 (1969)]; M. N. Rosenbluth and R. Z. Sagdeev, Comments Plasma Phys. Contr. Fusion 1, 129 (1972).

[3]R. J. Taylor, K. R. MacKenzie, and H. Ikezi, Rev. Sci. Instrum. 45, 1675 (1972).

[4]P. J. Barrett, D. Gresillon, and A. Y. Wong, in *Proceedings of the Third International Conference on Quiescent Plasmas, Elsinore, Denmark, 1971* (Jul. Gjellerups Forlag, Copenhagen, Denmark, 1971); A. S. Bakai, E. A. Kornilov, and S. M. Krivruchko, Pis'ma Zh. Eksp. Teor. Fiz. 12, 69 (1970) [JETP Lett. 12, 49 (1970)].

[5]T. M. O'Neil and J. H. Malmberg, Phys. Fluids 11, 1754 (1968).

[6]V. N. Oraevskii and R. Z. Sagdeev, Zh. Tech. Fiz. 32, 1291 (1962) [Sov. Phys. Tech. Phys. 7, 955 (1963)]; B. B. Kadomtsev, *Plasma Turbulence* (Academic, New York, 1965), p. 38.

[7]M. Porkolab and R. P. H. Chang, Phys. Fluids 13, 2054 (1970); M. N. Rosenbluth, R. B. White, and C. S. Liu, Phys. Rev. Lett. 31, 1190 (1973); R. Stenzel and A. Y. Wong, Phys. Rev. Lett. 28, 274 (1972).

[8]By measuring k_i/k_r, and using $\gamma/\omega = (V_g/V_{ph})(k_i/k_r)$.

[9]B. D. Fried, R. W. Gould, and G. Schmidt, University of California, Los Angeles, Plasma Physics Group Report No. R-146 (unpublished).

[10]A. Y. Wong and G. Schmidt, University of California, Los Angeles, Plasma Physics Group Report No. PPG-151 (unpublished).

[11]S. Kainer, J. Dawson, and T. Coffey, Phys. Fluids 15, 2419 (1972).

[12]Nonlinear Landau damping between electron waves has been observed by R. P. H. Chang and M. Porkolab [Phys. Rev. Lett. 25, 1262 (1970)] and K. W. Gentle and A. Malein [Phys. Rev. Lett. 26, 625 (1971)], and between ion waves by H. Ikezi and Y. Kiwamoto [Phys. Rev. Lett. 27, 718 (1971)].

Measurements of Plasma Density Distribution and Current-Sheath Structure in the Implosion Phase of a Theta-Pinch Discharge

K. F. McKenna, R. Kristal, and K. S. Thomas
University of California, Los Alamos Scientific Laboratory, Los Alamos, New Mexico 87554
(Received 26 December 1973)

The spatial and temporal evolution of the plasma density distribution and its relation to the magnetic-piston-field structure during a theta-pinch implosion have been experimentally investigated. With a deuterium fill density of 0.7×10^{15} atoms cm^{-3}, evidence of particle reflections from the imploding piston field is indicated.

The transient interaction between the imploding plasma and driving magnetic piston field in low-density ($10^{12} \leq n_0 \leq 6\times10^{13}$ cm^{-3}) fast-magnetic-compression θ-pinch devices has received considerable investigation.[1-3] In these experiments the implosion behavior can generally be described, depending on the density range, by either snowplow or free-particle models. However, in Scyllac-type devices[4] which operate at fill densities of approximately 10^{15} cm^{-3} the plas-